VII Jornades IdISBa

PÒSTERS DE L'ÀREA:

Oncologia i Hematologia

Institut d'Investigació Sanitària Illes Balears

IdISBa

VII Jornades IdISBa 2020

Epigenetic analysis of a model of Paired Glioma Stem Cells (GSC) and Non-Stem Glioma Cells (NSGC)

Miquel Ensenyat-Mendez, Sandra Íñiguez, Diego Marzese, and Borja Sesé

Cancer Epigenetics Lab, Cell Cancer Biology Group, Institut d'Investigació Sanitària Illes Balears (IdISBa)

Background and Rationale

Patients diagnosed with glioblastoma (GBM) have a median overall survival of only 15 months. One of the main factors affecting these patients' survival is the presence of a treatment-resistant population of cells, the Glioma Stem Cells (GSCs). These cells have stem cell-like properties, such as self-renewal and differentiation capacity to other GBM cell types. Furthermore, recent evidence manifest that these cells aggressive phenotype could be a result of epigenetic reprogramming. Here, we present a model of paired GSC and non-stem glioma cells (NSGCs), which have been epigenetically characterized to identify epigenetic regions that may be important for the maintaining of the stem-aggressive phenotype of GSCs

Methods

GSCs (HGCC 3035 and HGCC 3024 cell lines) were cultured in Neurobasal medium without serum. After five passages, these cells were transfered into RPMI medium with 10% serum to promote loss of stem phenotype, which was validated by qPCR markers (NESTIN). Then, paired GSCs and NSGCs were epigenetically characterized using EPIC DNA Methylation Array, and R was used to identify differentially methylated CpG sites (DMS). Finally, GREAT algorithm was used to identify genes located near DMS.

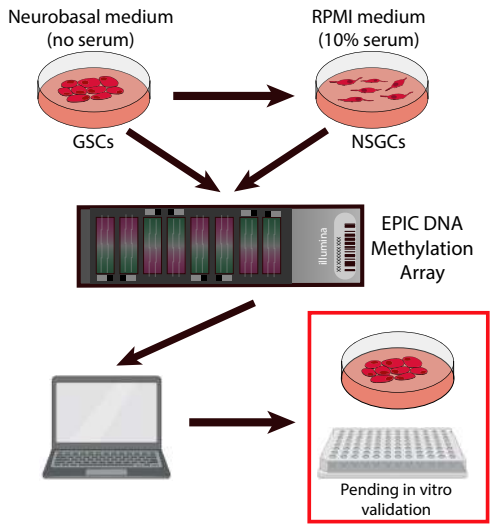

Figure 1. Schematic representation of methodology

Results

1- Identification of stemness markers

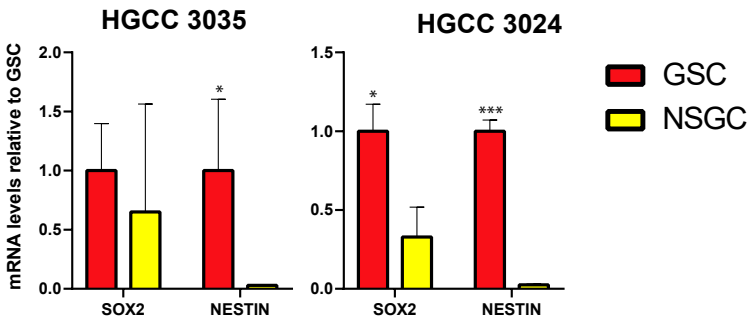

Figure 2. NESTIN mRNA levels are significantly higher in GSCs compared to NSGCs. SOX2 mRNA levels are significantly higher in GSC-3024 than NSGC-3024, but the change is not significant in 3035.

2- EPIC Array triplicates - Quality Analysis

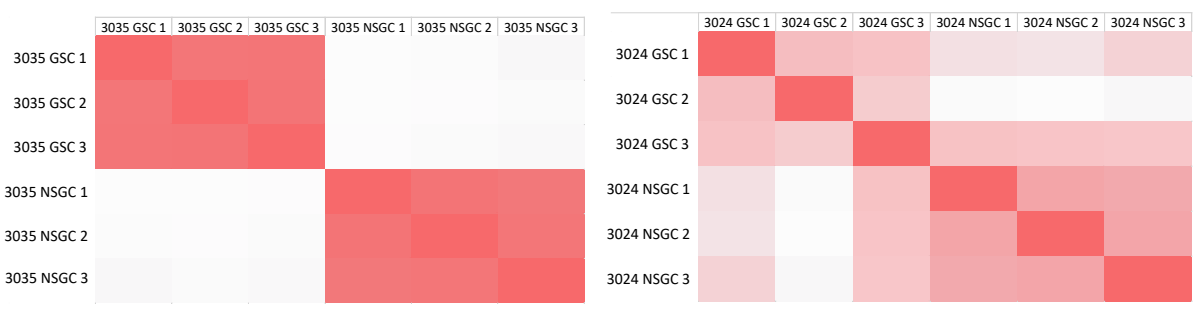

Figure 3. Correlation matrix heatmap of GSC and NSGC triplicates for HGCC 3035 and HGCC 3024 cell lines, respectively. The triplicates are highly correlated in 3035 GSC and NSGC, but only moderately correlated in both 3024 cell lines.

3- Identification of differentially methylated sites

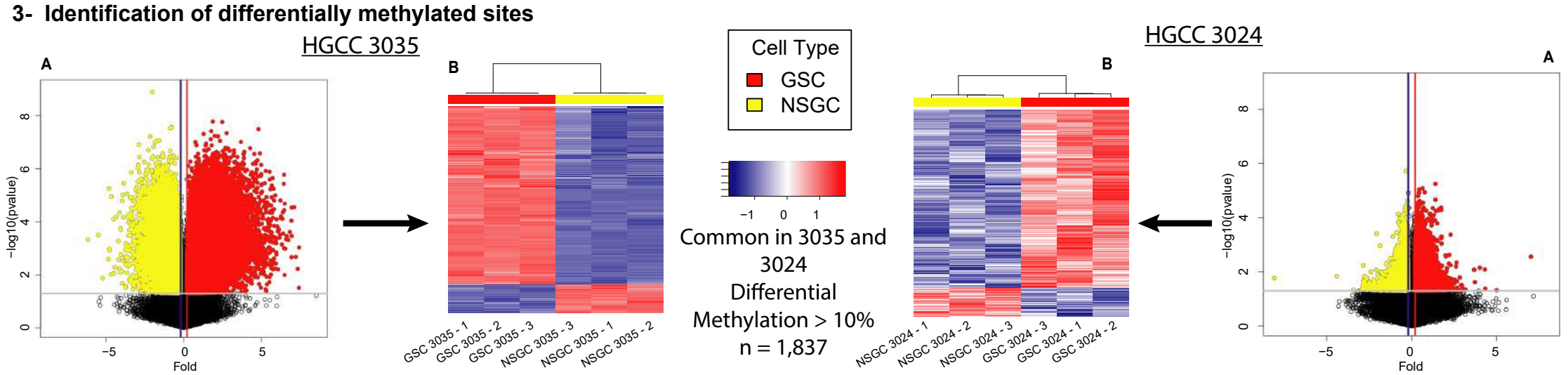

Figure 4. A) Volcano plot representing differential M-value, and q-value (FDR-corrected Student's t-test) for all analyzed CpG sites in GSC vs NSGC 3035. **B)** Heatmap representing hierarchical clustering of GSC and NSGC 3035 using all common DMS in 3035 and 3024 cell lines, with differential methylation over 10% (n = 1,837).

Figure 5. A) Volcano plot representing differential M-value, and q-value (FDR-corrected Student's t-test) for all analyzed CpG sites in GSC vs NSGC 3035. **B)** Heatmap representing hierarchical clustering of GSC and NSGC 3035 using all common DMS in 3035 and 3024 cell lines, with differential methylation over 10% (n = 1,837).

4- Description of genes near differentially methylated sites

More methylated in NSGCs

ZNF521

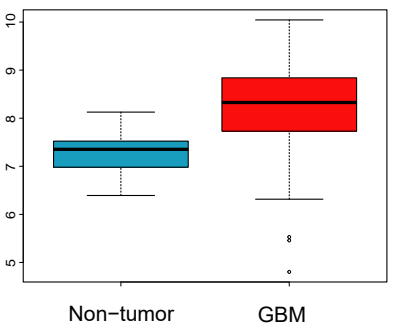

Figure 6. mRNA levels of ZNF521 iare significantly higher in GBM samples than in non-tumor brain samples (data obtained from GlioVis - Rembrandt cohort, p < 0.001)

- Stem cell associated co-factor
- Cooperates with GLI (glioma-associated transcription factor)

More methylated in GSCs

HTR1D

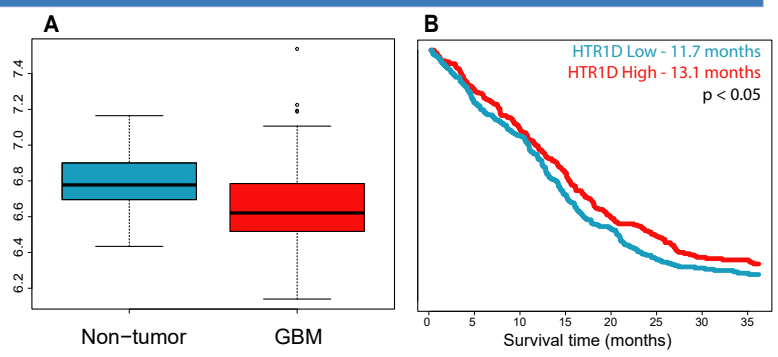

Figure 7. A) mRNA levels of HTR1D are significantly lower in GBM samples than in non-tumor brain samples (data obtained from GlioVis - Rembrandt cohort, p < 0.01). **B)** Kaplan-Meyer representation of GBM patients survival with high and low levels of HTR1D gene (cutoff = median).

Conclusions

We have generated the first epigenetic characterization of paired models of GSCs and NSGCs. This represents a unique resource for studying epigenetic determinants involved in the stem phenotype of glioma cells. Through mining of these datasets, we expect to identify potential relevance of various genes, which have been identified near several DMSs. These results lay the ground for the functional characterization of epigenetic alterations, which can be potentially relevant in the aggressive phenotype of the GSCs.

ESTUDIO DE LA EXPRESIÓN DE GENES ANTIOXIDANTES E INFLAMATORIOS EN LA FORMACIÓN DE MAMOSFERAS.

SASTRE-SERRA, Jorge[1,2]; MAROTO, Alba[1]; MUNAR, Margalida[3]; OLIVER, Jordi[1,2]; ROCA, Pilar[1,2] y PONS, Daniel Gabriel[1].

1 Grupo Multidisciplinar de Oncología Traslacional, Institut Universitari d'Investigació en Ciències de la Salut, Universitat de les Illes Balears (IUNICS), Instituto de Investigación Sanitaria Illes Balears (IdISBa)..

2 Ciber Fisiopatología Obesidad y Nutrición (CB06/03) Instituto Salud Carlos III, Madrid, Spain.

e-mail address: jorge.sastre@uib.es

INTRODUCCIÓN

El cáncer de mama puede desarrollarse siguiendo un modelo jerárquico de poblaciones de células heterogéneas con existencia de una pequeña subpoblación de células madre cancerosas (CSC) autoregenerables y poco diferenciadas. Estas CSCs son capaces de formar esferoides 3D en suspensión (mamosferas) en un medio definido sin suplementación con suero y cultivadas en placas de muy baja adherencia. La gran mayoría de la información publicada de procesos celulares proviene de experimentos llevados a cabo en condiciones adherentes o monocapa (2D), donde as interacciones célula-célula y célula-entorno extracelular no reflejan completamente la fisiología de la masa tumoral. Por el contrario, los esferoides 3D imitan mejor la arquitectura del tumor en condiciones fisiológicas y pueden usarse, no solo para estudios de farmacología, sino también para estudiar la biología de las células que inician el cáncer y los procesos de invasión y metástasis. En este sentido, nuestro objetivo fue estudiar la expresión génica relacionada con marcadores de CSC, el estrés oxidativo y la inflamación en mamosferas en comparación con cultivos adherentes de la línea celular de cáncer de mama MCF7.

MATERIALES Y MÉTODOS

Para llevar a cabo el estudio se sembraron células MCF7 con medio de crecimiento de mamosferas (3D Tumorsphere Medium XF, Promocell) en placas de cultivo celular (2D) y en placas con muy baja adherencia (3D) para la obtención de mamosferas. Se realizó el aislamiento y retrotranscripción del ARN y qPCR en tiempo real para analizar la expresión de ARNm relacionados con marcadores de CSC, el estrés oxidativo y la inflamación.

RESULTADOS

Al estudiar la expresión génica de marcadores asociados a CSCs, se observó una disminución de la expresión de sox2 y un aumento en nanog en comparación con el cultivo 2D. Al comparar el cultivo de mamosferas (3D) con el cultivo en 2D se observó un incremento en la expresión génica de sod1,sod2 y nrf2, así como una disminución de los niveles de ARNm de sirt3 y ucp2. Además, el cultivo de mamosferas presentó un incremento de la expresión de los genes proinflamatorios nf-kb, il8, il6 e il6r, así como una disminución de la expresión del gen anti-inflamatorio TGFb.

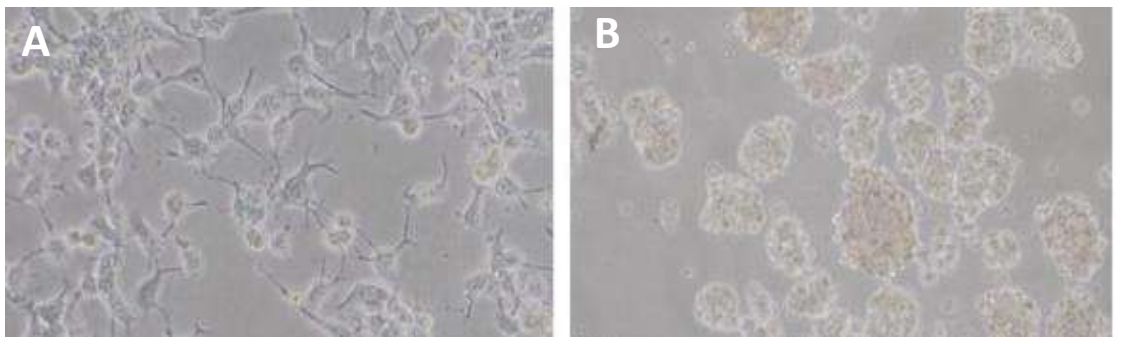

Figura 1. Morfología línea celular MCF7 en cultivo 2D y 3D. Fotografías (63x) de células MCF-7 después de 24h de cultivo en placas adherentes (A) y en placas de muy baja adherencia (B) con medio 3D Tumorsphere Medium (Promocell).

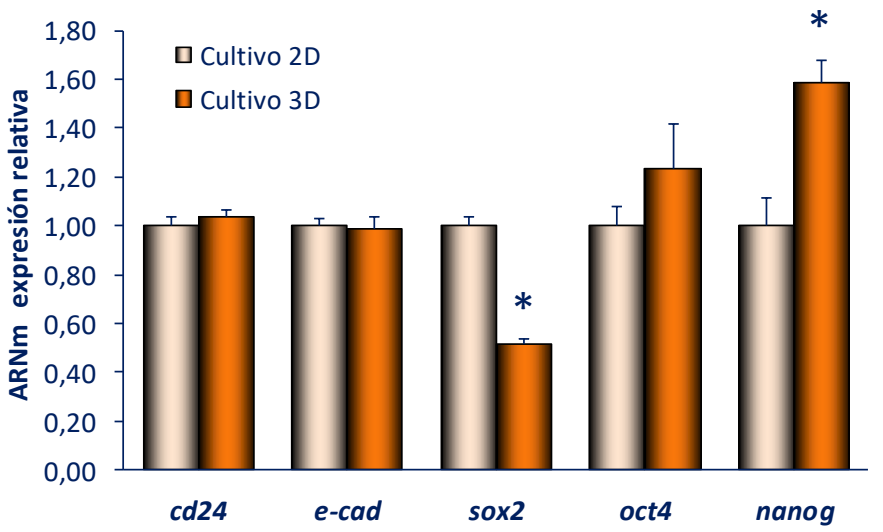

Figura 2. Expresión génica de marcadores asociados a CSCs en MCF7 en cultivo 2D y 3D. Detección de los niveles de ARNm de cd24, e-cad, sox2, oct4 y nanog en células MCF7 después de 24h de cultivo en placas adherentes (2D) y en placas de muy baja adherencia (3D) con medio 3D Tumorsphere Medium (Promocell). La expresión génica fue relativizada a los niveles de ARNm de 6 genes *housekeeping*: tbp, ywhaz, hmbs, ppia, 18s, b2m y actb. Los valores se representan como la media ± SEM (n=6). * Diferencia significativa entre 2D y 3D (p<0,05(t-Student)).

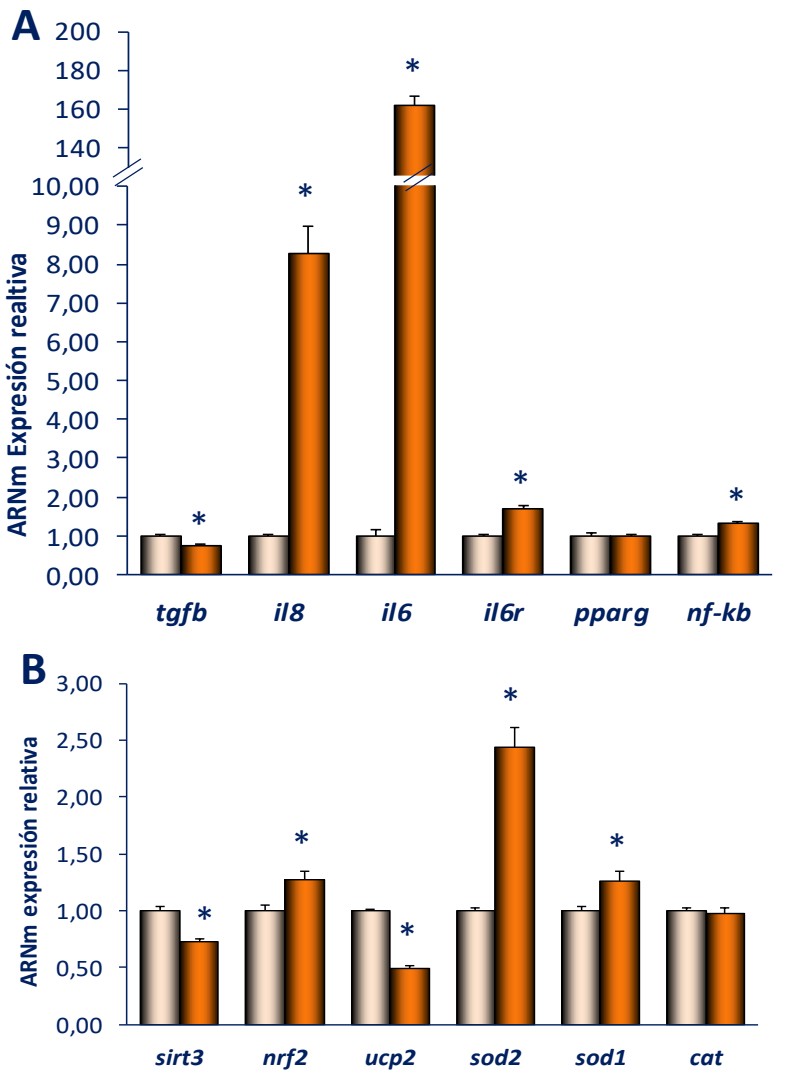

Figura 3. Expresión génica de genes relacionados con el estrés oxidativo y la inflamación en MCF7 en cultivo 2D y 3D. Detección de los niveles de ARNm de tgfb, il8, il6, il6r, pparg y nf-kb (A); así como de srit3,nrf2, upc2, sod2, sod1 y cat (B) en células MCF7 después de 24h de cultivo en placas adherentes (2D) y en placas de muy baja adherencia (3D) con medio 3D Tumorsphere Medium (Promocell). La expresión génica fue relativizada a los niveles de ARNm de 6 genes *housekeeping*: tbp, ywhaz, hmbs, ppia, 18s, b2m y actb. Los valores se representan como la media ± SEM (n=6). * Diferencia significativa entre 2D y 3D (p<0,05(t-Student)).

CONCLUSIONES

La formación de mamosferas en la línea celular MCF7 modifica la expresión de genes relacionados con el estrés oxidativo y la inflamación. Las mamosferas presentarían un estado de estrés oxidativo e inflamación que podría beneficiar a las células que forman las mamosferas (CSCs) a adquirir un fenotipo más agresivo y proliferativo. Aún así, cabe destacar que los resultados obtenidos en maradores asociados a CSCs, indican que las mamosferas primarias son una población heterogénea formada por agregados celulares en los que el porcentaje de CSCs puede variar.

AGRADECIMIENTOS

Proyecto financiado por "Un lazo en movimiento (ULEM)" a través del IdISBa.

LA GENISTEÏNA A ALTES CONCETRACIONS INCREMENTA L'ESTRÈS OXIDATIU I LA INFLAMACIÓ EN CÈL·LULES DE CÀNCER DE COLON

Alorda-Clara M[1], Gaya-Bover A[1], Castell-Sanmartin N[1], Reyes J[1], Roca P[1,2], Sastre-Serra J[1,2], Pons DG[1], Oliver J[1,2]

[1] Grup Multidisciplinar d'Oncologia Traslacional, Institut Universitari d'Investigació en Ciències de la Salut (IUNICS), Universitat de les Illes Balears, Institut d'Investigació Sanitària de les Illes Balears (IdISBa).

[2] Centro de Investigación Biomédica en Red Fisiolpatología de la Obesidad y la Nutrición (CIBERObn, CB06/06), ISCIII.

INTRODUCCIÓ

La genisteïna és un fitoestrogen que té efectes sobre la regulació de l'estrès oxidatiu, la biogènesi mitocondrial i la inflamació, tres processos fisiològics íntimament lligats, que es troben alterats en el càncer. No obstant això, el paper de la genisteïna en el càncer colorectal encara no es troba completament determinat.

El nostre objectiu va ser determinar els efectes de la genisteïna sobre aquests tres processos a dues línies cel·lulars de càncer de colon: HT29 i SW60

MATERIALS i MÈTODES

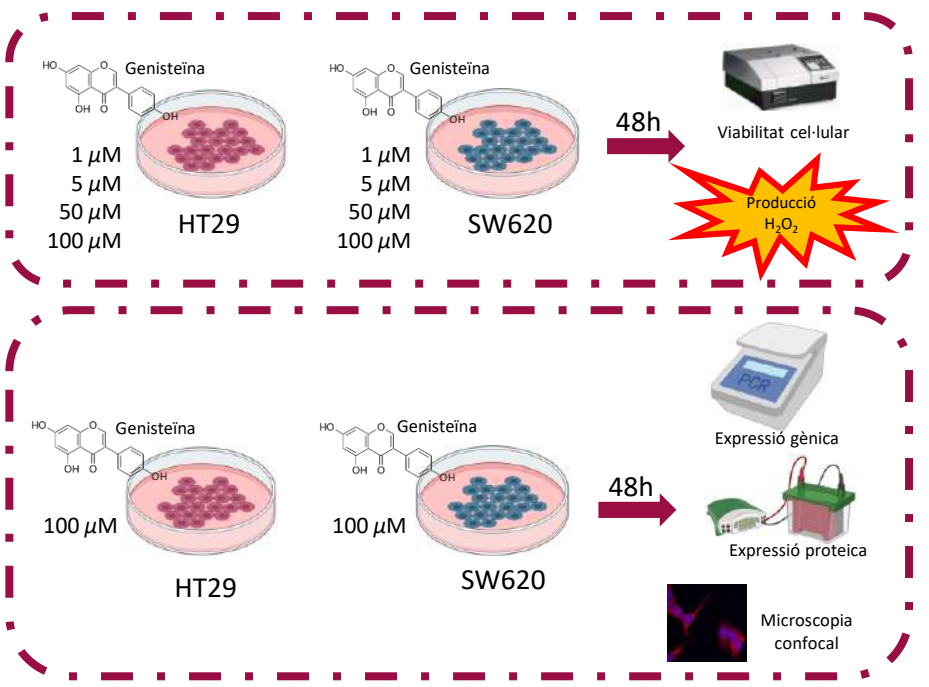

RESULTATS

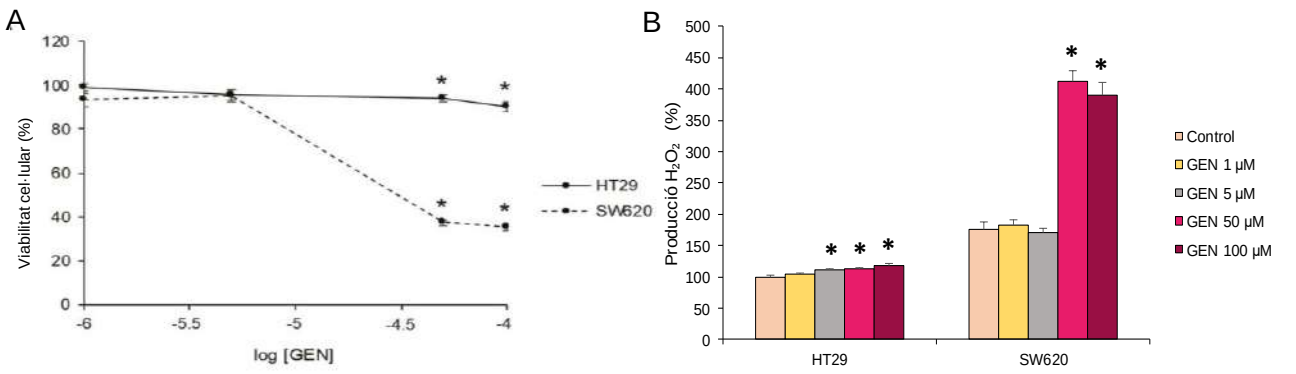

Figura 1. Efecte de diferents concentracions de genisteïna (1, 5, 50 i 100 μM) a HT29 i SW620. **A** Efectes sobre la viabilitat cel·lular, determinada per Hoechst 33342. **B** Efectes sobre la producció de H_2O_2, determinada per l'assaig Amplex® Red Hydrogen Peroxide/Peroxidase. Els resultats s'expressen com mitja ± SEM i estan normalitzats com a percentatge de les cèl·lules control HT29 (0,1% DMSO). * diferències significatives entre control i genisteïna (N=6; t-Student P < 0,05).

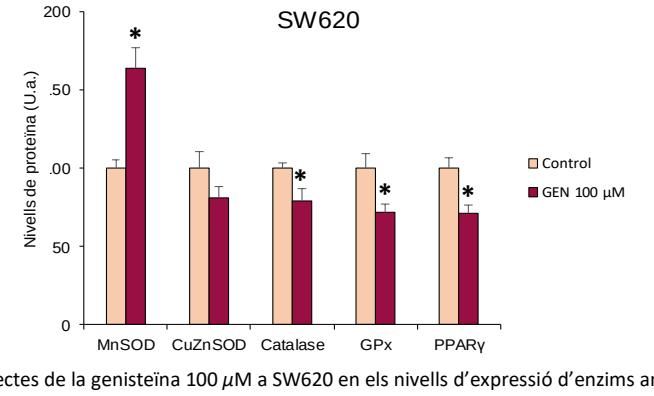

Figura 2. Efectes de la genisteïna 100 μM a SW620 en els nivells d'expressió d'enzims antioxidants i proteïnes anti-inflamatòries, determinats per Western blot. Els valors s'expressen com mitja ±SEM, les cèl·lules control (0,1% DMSO) s'expressen com a 100. * diferències significatives entre control i genisteïna (N=6; t-Student P < 0,05).

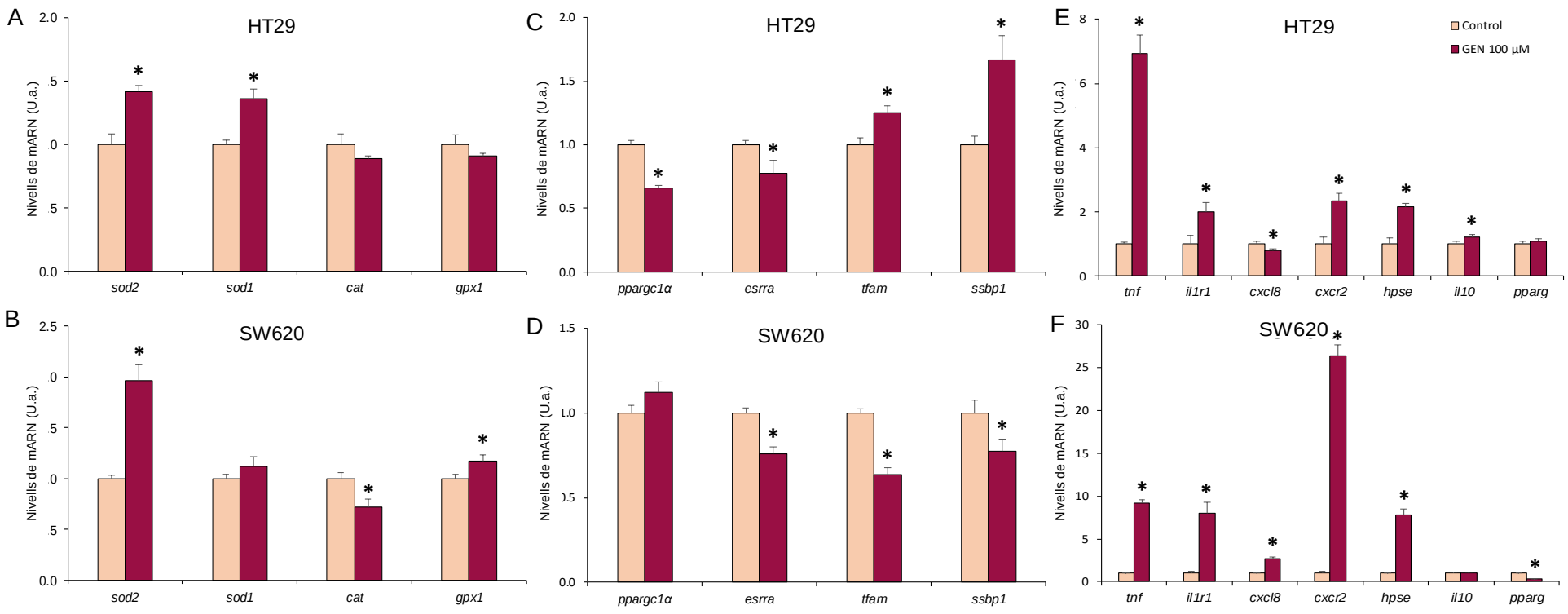

Figura 3. Efectes de la genisteïna 100 μM a HT29 (**A**, **C**, **E**) i SW620 (**B**, **D**, **F**) sobre els nivells d'expressió de mRNA d'enzims antioxidants (**A**, **B**), gens relacionats amb la biogènesi mitocondrial (**C**, **D**) i gens relacionats amb la inflamació (**E**, **F**), determinats per PCR a temps real. Els valors s'expressen com a mitja ± SEM, les cèl·lules control (0,1% DMSO) s'expressen com a 1. * diferències significatives entre control i genisteïna (N=6; t-Student P < 0,05).

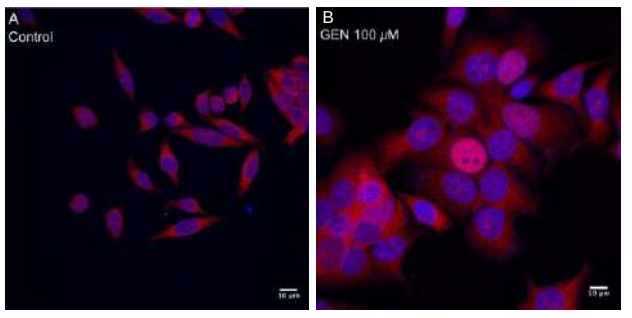

Figura 4. Efecte de la genisteïna 100 μM sobre la translocació de NFκB a les cèl·lules SW620 determinada per inmunocitoquímica. **A** Cèl·lules SW620 control (0,1% DMSO), **B** cèl·lules SW620 tractades amb genisteïna. Nuclis representats de color blau i proteïna NFκB en vermell; la superposició d'ambdós colors indica la translocació de NFκB dins el nucli.

CONCLUSIÓ

La genisteïna a altes concentracions promou un increment de l'estrès oxidatiu degut al descens dels nivells d'expressió d'enzims antioxidants i, a SW620, a l'acumulació de mitocondris poc funcionals, provocat pel descens dels nivells de biogènesi mitocondrial. Aquest estrès oxidatiu està directament relacionat amb l'increment dels nivells d'inflamació, la qual cosa provocaria un descens de la viabilitat cel·lular, especialment a la línia cel·lular SW620.

Agraïments

Fondo de Investigaciones Sanitarias del Instituto de Salud Carlos III (PI14/01434) Gobierno de España, confinançat per FEDER-Unión Europea ("Una manera de hacer Europa"). Unitat de celòmica (IUNICS).

Uncovering immune-evasive mechanisms of a novel glioma stem cell population: new insights for glioblastoma immunotherapy

VII Jornades IdISBa 2020

Íñiguez-Muñoz, S.; Ensenyat-Mendez, M.; Bennasar-Roman, M.; Marzese, DM.; Sesé, B.

Cancer Epigenetics Lab, Cancer Biology Group, Institut d'Investigació Sanitària Illes Balears (IdISBa)

BACKGROUND

Glioblastoma (GBM) is the most common and deadly primary brain tumor with an extremely poor prognosis. Glioma stem cells (GSCs) play a significant role in GBM growth and relapse. This small cell population is thought to be responsible for GBM tumor resistance and immune evasion abilities. However, there is some controversy regarding the isolation and expansion of GSCs in vitro. Using publicly available single-cell RNAseq data, we have identified a novel population of GSCs, hereinafter called core-GSCs (c-GSCs), which presents high expression levels of the embryonic stem cell (ESC) markers OCT4, SOX2, and NANOG, together with a dramatic downregulation of antigen presentation HLA genes (**Figure 1**). Here, we have generated glioma-induced pluripotent stem cells (GiPSCs) as an in vitro model that recapitulates the transcriptomic profile and precursor state of the c-GSCs population. We plan to use our GiPSC model to identify gene regulatory mechanisms governing GBM immune evasion. Overall, these findings could lead to novel and more effective strategies for immunotherapy in GBM.

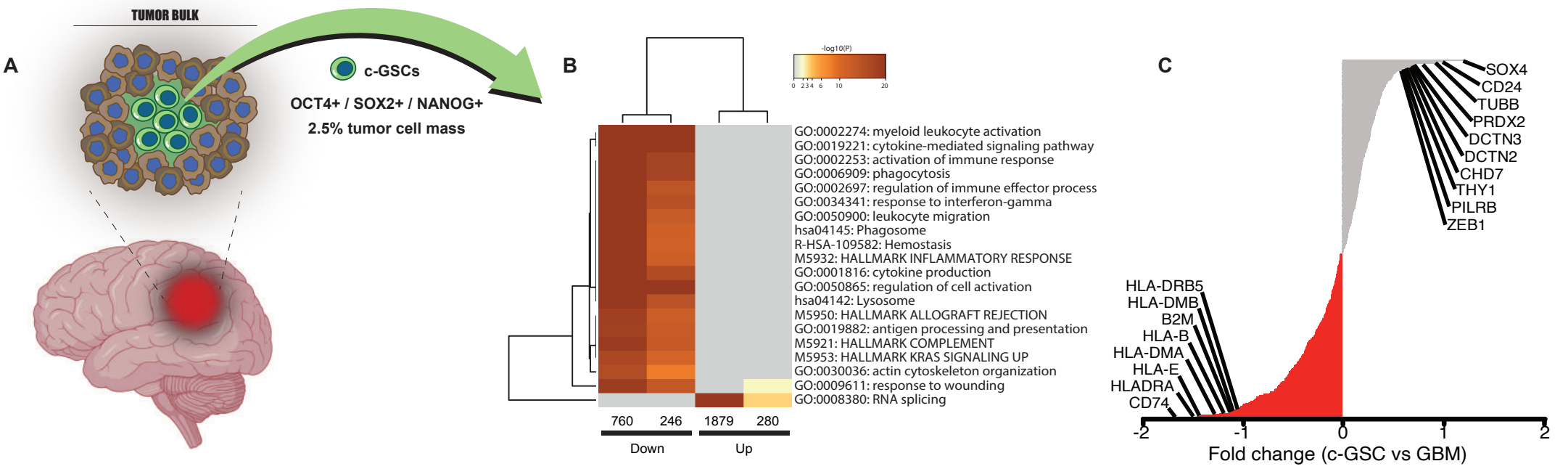

Figure 1. A) c-GSCs present high levels of ESC markers OCT4, SOX2, and NANOG and represent 2.5% of the tumor cell mass. B) Gene Set Enrichment Analysis in c-GSCs. C) Transcriptomic analysis of differentially expressed genes in c-GSCs compared to GBM tumor bulk cells.

METHODS

GiPSCs were derived from conventional GSCs using a lentivirus carrying the reprogramming factors OCT4, SOX2, KLF4, and MYC in a single polycistronic vector. GSCs were cultured in Neurobasal serum-free media. GiPSCs colonies appeared after four weeks cultured in mTeSR1 media, and single-cell clones were manually generated in a 96-well plate. Total RNA was extracted from GSCs and GiPSCs, reverse transcribed into cDNA, and gene expression analysis was performed by qPCR. Immunofluorescence analyses were performed in GSCs and GiPSCs and stained with antibodies against OCT4, SOX2, NANOG, and HLA-ABC.

RESULTS

Figure 2. A) Gene expression analysis revealed that GiPSCs present high expression of pluripotency markers OCT4, SOX2 and NANOG, similar to our newly identified c-GSC population in GBM (left). In concordance with the transcriptomic profile of c-GSC shown in Figure 1C, GiPSCs also present low levels of HLA-B, and high levels of SOX4 compared to GSCs (right). Statistics: *$p < 0.05$; **$p < 0.01$

B) Immunofluorescence analysis confirmed the expression of OCT4, SOX2, and NANOG in GiPSC colonies together with a strong downregulation of MHC Class I proteins HLA-A, -B, and -C.

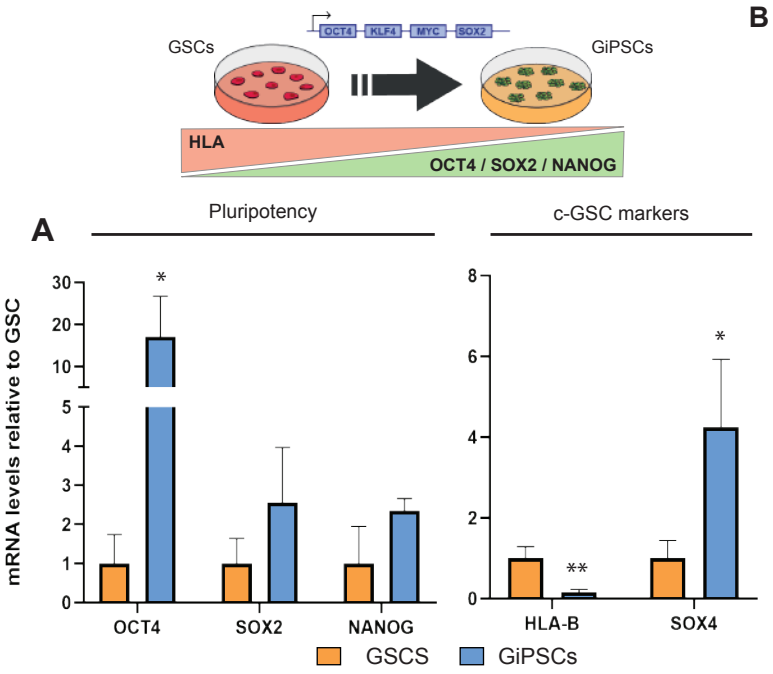

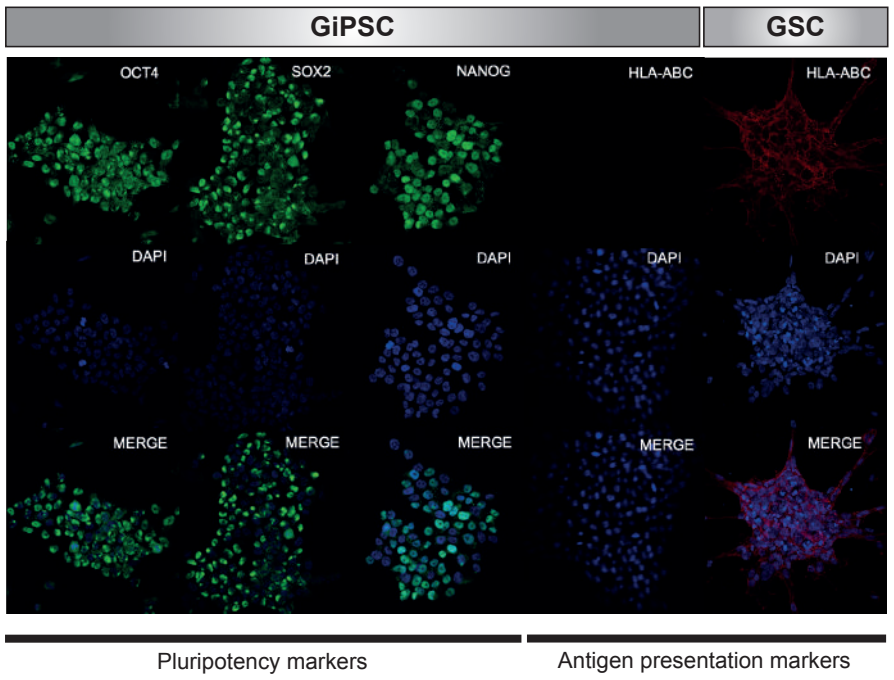

CONCLUSIONS

Here we present c-GSCs as a novel GSC population in GBM, exhibiting ESCs pluripotency markers and a significant loss of antigen presentation via HLA downregulation. Our findings showed that GiPSCs mimic the c-GSC phenotype in vitro, both at mRNA and protein levels. Thus, GiPSCs can become an excellent model to study the underlying mechanism responsible for immune evasion in GBM and explores other critical areas such as drug resistance, tumor growth and tumor microenvironment.

IMPORTANCIA DE LA DINÁMICA MITOCONDRIAL EN EL CÁNCER DE MAMA. PAPEL DEL RECEPTOR DE ESTRÓGENOS BETA EN UNA SITUACIÓN DE INFLAMACIÓN ASOCIADA A LA OBESIDAD

MARTINEZ-BERNABE, Toni[1], CIOBU, Nicolae[1], OLIVER, Jordi[1,2], PONS, Daniel Gabriel[1], ROCA, Pilar[1,2], SASTRE-SERRA, Jorge[1,2].

1 Grupo Multidisciplinar de Oncología Traslacional, Institut Universitari d'Investigació en Ciències de la Salut (IUNICS), Universitat de les Illes Balears (IdISBa), 07122 Palma, Spain. Instituto de Investigación Sanitaria Illes Balears, 07010 Palma, Spain.

2 Ciber Fisiopatología Obesidad y Nutrición (CB06/03) Instituto Salud Carlos III, Madrid, Spain. e-mail address: jorge.sastre@uib.es

INTRODUCCIÓN

El desarrollo y la progresión del cáncer de mama podrían verse incrementados por los estrógenos, leptina y citoquinas inflamatorias que el tejido adiposo produce. En estos procesos, la dotación de receptores de estrógenos ERα/ERβ adquiere un papel relevante, siendo un factor determinante en la respuesta celular en el cáncer de mama. El objetivo de este estudio ha sido analizar el papel de la ratio de receptores estrogénicos ERα/ERβ sobre la mitocondria en una situación de inflamación asociada a la obesidad en líneas celulares de cáncer de mama.

MATERIALES Y MÉTODOS

Se estudiaron los efectos del tratamiento con estrógenos (10 nM), leptina (100 ng/ml), IL-6 (50 ng/ml) y TNF-α (10 ng/ml) sobre dos líneas celulares de cáncer de mama: MCF7 (mayor ratio ERα/ERβ) y T47D (menor ratio ERα/ERβ). Para ello se analizaron la expresión génica de enzimas antioxidantes, biogénesis y dinámica mitocondriales (qPCR) y la producción de H_2O_2 (Fluorimetría), los niveles proteicos de enzimas antioxidantes, complejos OXPHOS y el daño oxidativo (Western blot).

RESULTADOS

La biogénesis mitocondrial tras el tratamiento en la línea MCF7 mostró menores niveles de ARNm de PPARGC1A, ERRa, NRF1, TFAM, Twinkle y mtSSB. Por otro lado, la línea T47D presentó un aumento de la expresión de ESRRA y Twinkle. Los niveles proteicos del sistema OXPHOS disminuyeron en la línea MCF7 y no en T47D, tras el tratamiento. Los marcadores de dinámica mitocondrial MFN1, MFN2, OPA1, OMA1, DRP1 y FIS1, presentaron una disminución de su expresión génica en la línea MCF7 tras el tratamiento, sin embargo, ocurre lo contrario en la línea T47D. La producción de H_2O_2 aumentó especialmente en la línea celular MCF7 (200 ± 8%). Las células MCF7 tratadas incrementaron los niveles de expresión proteica de MnSOD (1631 ± 552%), mientras que disminuyeron los de Catalasa y GRd. La línea T47D incrementó la expresión proteica tanto de MnSOD como de CuZnSOD. La línea MCF7 mostró un mayor daño oxidativo lipídico tras el tratamiento (145 ± 8%), mientras que no ocurrió lo mismo en la línea T47D.

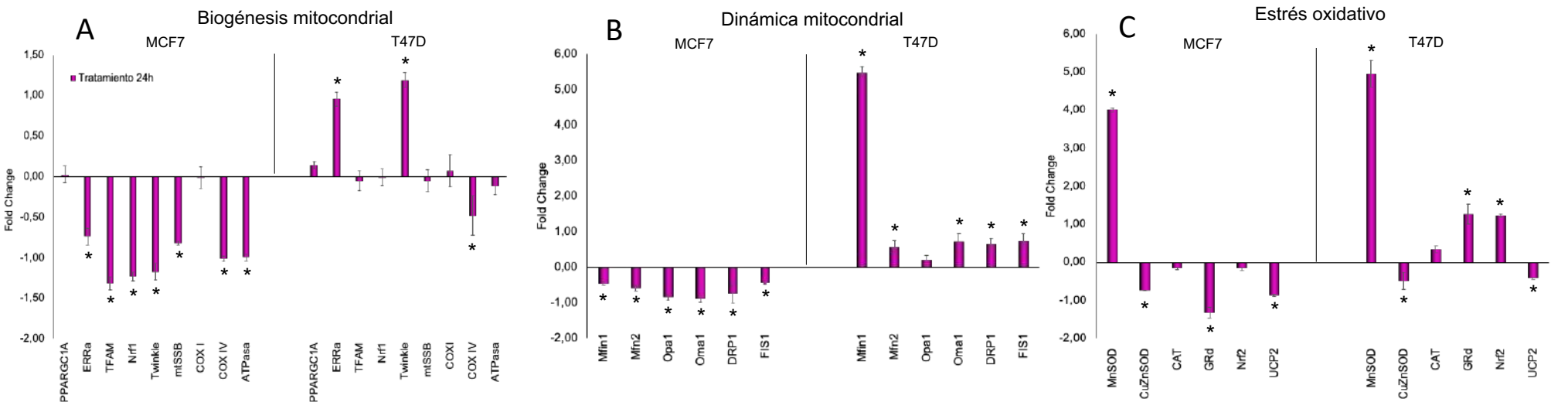

*Figura 1. Efecto del tratamiento con estrógenos, leptina, IL-6 y TNF-α sobre la expresión génica de genes implicados en la biogénesis mitocondrial (A), la dinámica mitocondrial (B) y el estrés oxidativo (C). *: Diferencia significativa tras el análisis estadístico con t-student (p<0,05). (MCF-7 n=3 y T47D n=6)*

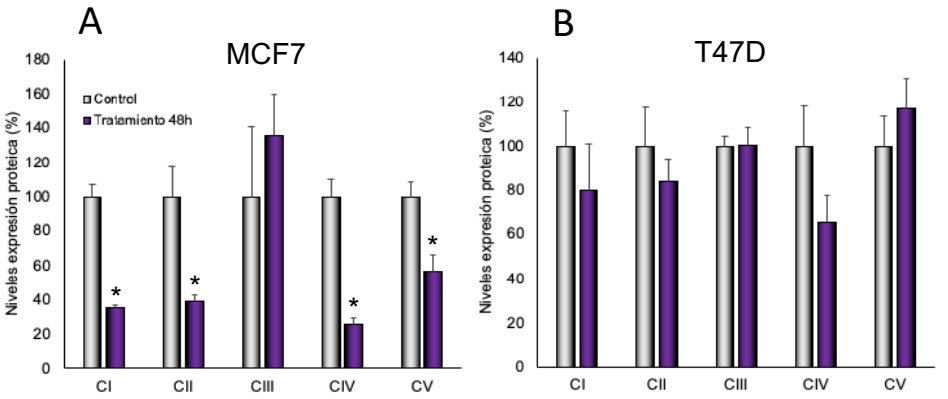

*Figura 2. Efecto del tratamiento con estrógenos, leptina, IL-6 y TNF-α sobre los niveles proteicos de OXPHOS en las líneas MCF7 (A) y T47D (B). *: Diferencia significativa tras el análisis estadístico con t-student (p<0,05). (MCF-7 n=3 y T47D n=3)*

*Tabla 1. Efecto del tratamiento con estrógenos, leptina, IL-6 y TNF-α sobre la producción de H2O2, daño oxidativo y niveles proteicos de enzimas antioxidantes. *: Diferencia significativa tras el análisis estadístico con t-student (p<0,05). (MCF-7 n=6 y T47D n=6)*

	MCF-7		T47D	
	Control	Tratamiento	Control	Tratamiento
Producción H_2O_2 (%)	100 ± 1	200 ± 8*	100 ± 3	134 ± 3*
Daño oxidativo (%)	100 ± 5	145 ± 8*	100 ± 7	92,3 ± 11,7
Niveles proteicos de MnSOD (%)	100 ± 11	1631 ± 552*	100 ± 15	3691 ± 350*
Niveles proteicos de CuZnSOD (%)	100 ± 12	89,1 ± 14,1	100 ± 25	156 ± 28
Niveles proteicos de Catalasa (%)	100 ± 6	69,9 ± 7,8	100 ± 14	88,2 ± 10,0
Niveles proteicos de GRd (%)	100 ± 14	49,5 ± 6,0*	100 ± 9	117 ± 8

CONCLUSIONES

La línea MCF7, con una mayor ratio ERα/ERβ, mostró un decrecimiento de la biogénesis mitocondrial y la dinámica mitocondrial ante un tratamiento inflamatorio asociado a la obesidad, mientras que la línea T47D, con una menor ratio ERα/ERβ, muestra pocos cambios en la biogénesis mitocondrial, aunque aumenta la dinámica mitocondrial. Estos datos correlacionan con el estrés oxidativo observado en las líneas celulares, donde la línea MCF7 muestra un incremento en el estrés oxidativo tras el tratamiento de inflamación asociada con la obesidad, lo cual se traduce en daño oxidativo. Por otro lado, la línea T47D no presentó daño oxidativo, en parte, debido al mantenimiento de los niveles de enzimas antioxidantes y un pool de mitocondrias más funcionales. Estos estudios sugieren que ERβ podría tener un rol importante manteniendo la dinámica mitocondrial, evitando así un mayor daño oxidativo en una situación de inflamación y obesidad en cáncer de mama.

AGRADECIMIENTOS

Este trabajo ha sido financiado por la Fundació Institut d'Investigacio Sanitària Illes Balears (IdISBa) - Proyectos intramurales Programa "Primus" 2018 (PRI18/04).

Proyecto Investigacón en Cáncer de Mama (InCaM), Fundació Universitat Empresa de les Illes Balears (FUEIB) – Oficina de Fundraising. Feim Cami per Viure – Santa Maria del Camí.

Potencial coadyuvante de las fenotiazinas antipsicóticas en glioblastoma: estudio del papel de FOXO3a

Lucía Ferro[1,3], Guillem Ramis[1,3,4], Priam Villalonga[1,2,3], Silvia Fernández de Mattos[1,2,3]

[1]Grupo de Biología Celular del Cáncer, IUNICS, [2]Departamento de Biología Fundamental y Ciencias de la Salud, Universidad de las Islas Baleares (UIB),

[3]Instituto de Investigación Sanitaria Illes Balears (IdISBa), Palma, Illes Balears (España), [4] Unidad de Celómica, IUNICS-UIB

Antecedentes

Nivel clínico

El **glioblastoma** (GBM) es la manifestación clínica más agresiva de los tumores del sistema nervioso central[1].

Los pacientes acaban siendo resistentes al **tratamiento convencional**, que implica una resección quirúrgica seguida de radioterapia y/o quimioterapia con temozolomida (TMZ)[2].

Nivel molecular

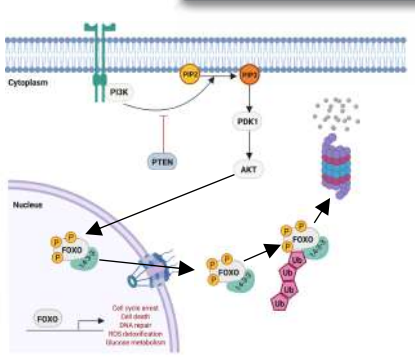

Figura 1. Vía de señalización PI3K-AKT-FOXO3a.

Un 88% de los GBM presentan alterada la vía de señalización **PI3K-AKT-mTOR**. Como consecuencia el supresor tumoral **FOXO3a** es exportado del núcleo e inactivado[3].

Necesidad de una nueva estrategia terapéutica

Drug repositioning

Fenotiazinas antipsicóticas

Clorpromazina (CPZ) | Tioridazina (TRD)

Objetivos

Evaluar el potencial adyuvante de las fenotiazinas antipsicóticas (TRD y CPZ) en combinación con TMZ en células de GBM.

Estudiar el efecto celular de las fenotiazinas antipsicóticas en GBM.

Materiales y métodos

Líneas celulares de GBM LN229, U87MG, U251 y cultivos primarios derivados de pacientes (P#04, P#23).

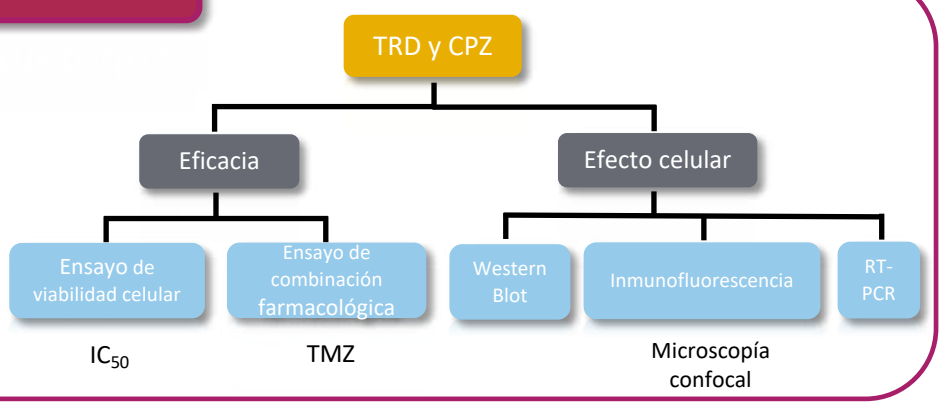

Resultados

Viabilidad celular y potencial adyuvante

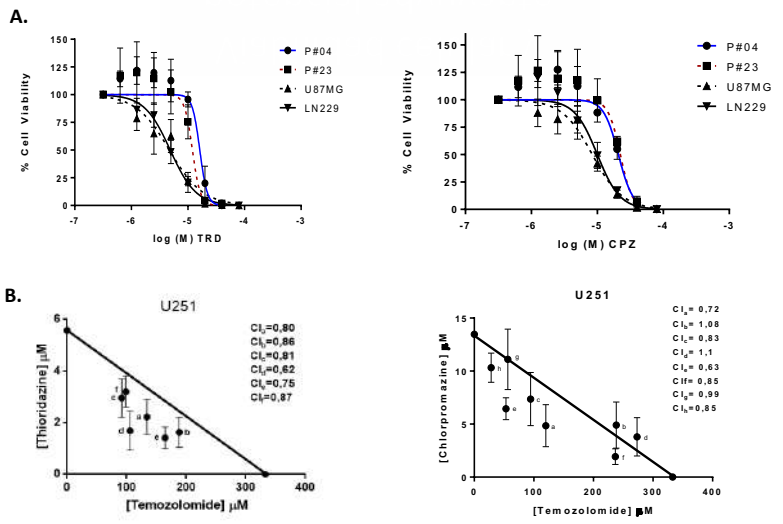

Figura 2. Las fenotiazinas antipsicóticas (TRD y CPZ) reducen la viabilidad celular y presentan efectos sinérgicos en combinación con TMZ, en líneas celulares humanas de GBM y en cultivos primarios de GBM. (A) Curvas dosis-respuesta de TRD y CPZ. Las líneas celulares indicadas fueron tratadas con diluciones seriadas 1:2 de los fármacos, a partir de una concentración mayor de 20 µM. (B) Efecto de la combinación de TRD y CPZ en combinación con TMZ en U251. Las células de GBM fueron tratadas con los fármacos a ratios de combinación fijas (1:1, 1:2, 2:1, 1:3, 3:1, 1:5, 5:1, 1:10 y 10:1). Los datos que se muestran en los isobologramas corresponden a las medias ± SD de dos experimentos independientes.

Efecto celular

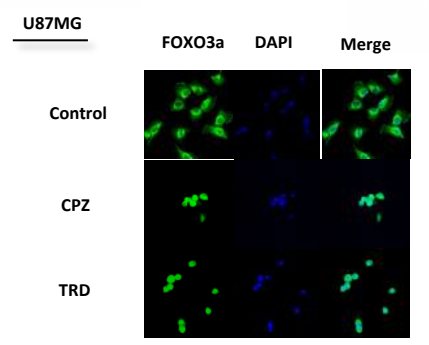

Figura 3. TRD y CPZ inducen la acumulación nuclear de FOXO3a. Las células de GBM crecieron sobre cubreobjetos y fueron tratadas con TRD o CPZ a 10 µM durante 3h, a excepción de las células control. Seguidamente fueron fijadas y marcadas con el anticuerpo *anti-FOXO3a* (verde) y los núcleos con *DAPI* (azul).

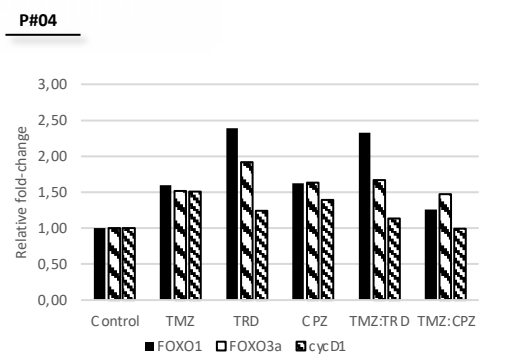

Figura 4. TRD, CPZ y TMZ Inducen la expresión de FOXO3a, FOXO1 y de ciclina D1, solos o en combinación. Análisis por RT-PCR de los niveles de expresión de FOXO1, FOXO3a y ciclina D1 en células de paciente (P#04). Las células fueron tratadas a dosis concretas y fueron recogidas a las 2h de tratamiento.

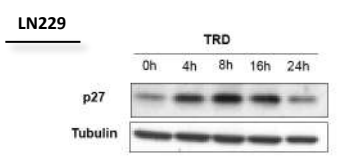

Figura 5. TRD induce un incremento de los niveles proteicos de p27 de manera tiempo dependiente. Análisis por *Western-Blot* de la proteína p27 en la línea celular LN229. Esta línea celular de GBM fue tratada con TRD a 10 µM a diferentes tiempos (4h, 8h, 16h y 24h). α-tubulina fue utilizada como control de carga.

Conclusiones

1. Las fenotiazinas antipsicóticas disminuyen la viabilidad celular de las células de GBM.
2. La combinación de TMZ con las fenotiazinas antipsicóticas (CPZ y TRD) resulta sinérgica en un gran número de combinaciones.
3. Las fenotiazinas antipsicóticas promueven la importación nuclear de FOXO3a y lo activan, ya que modulan la expresión de genes diana de FOXO3a como FOXO1, ciclina D1 y p27.
4. Estos resultados sugieren el potencial de las fenotiazinas antipsicóticas TRD y CPZ como tratamiento adyuvante del GBM.

Referencias bibliográficas

1. Maher, E. A. *et al.* Malignant glioma: genetics and biology of a grave matter. *Genes Dev.* **15**, 1311–1333 (2001).
2. Friedman, H. S., Kerby, T. & Calvert, H. Temozolomide and Treatment of Malignant Glioma. *Clin. Cancer Res.* **6**, (2000).
3. Fruman, D. A. *et al.* The PI3K Pathway in Human Disease. *Cell* **170**, 605–635 (2017).

Las imágenes fueron diseñadas con la página web Biorender.

Cuestiones y comentarios: lucia.ferro@uib.es

Characterization of druggable Wnt pathway molecular alterations in patient-derived cultures for evaluation of new soft tissue sarcoma therapies

Marina Pérez-Capó[1,2], Esther Martinez-Font[1,2] , Elena Prados[3], Rafael Ramos[3], Raúl Sánchez[2], Regina Alemany[1,4], Antònia Obrador-Hevia[1,5].

[1]Group of Advanced Therapies and Biomarkers in Clinical Oncology, Institut d'Investigació Sanitària Illes Balears (IdISBa), Palma de Mallorca, Spain; [2]Medical Oncology Department, Hospital Universitari Son Espases, Palma de Mallorca, Spain; [3]Pathology Department, Hospital Universitari Son Espases, Palma de Mallorca, Spain; [4]Group of Clinical and Translational Research, Department of Biology, University of the Balearic Islands, Palma de Mallorca, Spain; [5]Molecular Diagnosis Unit, Son Espases University Hospital, Palma de Mallorca, Spain.

Introduction

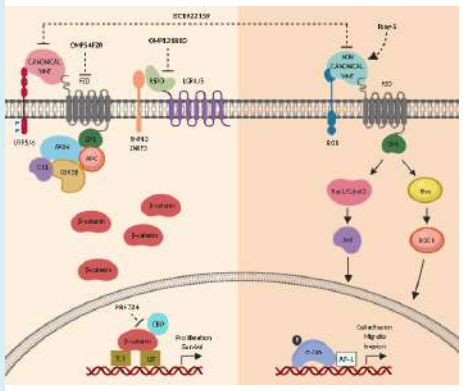

Canonical and non-canonical Wnt signalling pathways and Wnt pathway inhibitor drugs in clinical trials.

Soft tissue sarcomas (STS) are malignant tumours of mesenchymal origin with 50 different histological subtypes which represent 1 % of all solid malignant neoplasia in adults. The poor prognosis of STS (5-year survival of 16% in patients with disseminated disease) makes the development of new therapeutic approaches based on personalized medicine with clearly defined biomarkers a capital need. In this context, Wnt signalling pathway involved in crucial processes during development and tissue homeostasis has been found to have aberrant activation in many cancers, including STS. Our research group has preliminary published data which point to a role of the Wnt signaling pathway as a therapeutic target that could complement current STS treatments. Despite this, its involvement in sarcomagenesis has not yet been exhaustively studied.

The aims of this project were: 1) to identify molecular alterations of the Wnt signalling pathway in STS by exploiting public genomic data and in a wide range of patient samples; 2) to set up a protocol for the establishment of patient-derived primary cultures as a model for validation of these Wnt alterations and test targeted therapies against them.

Methodology

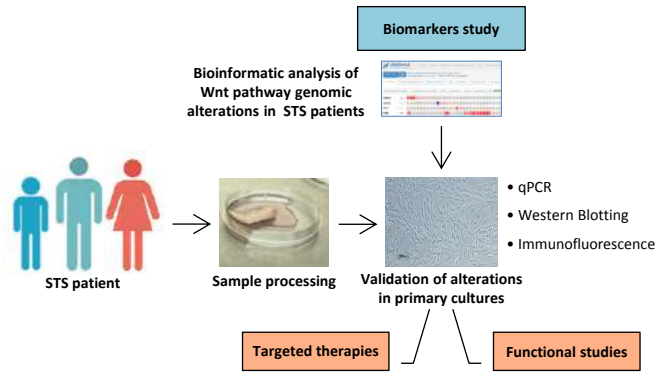

Figure 1. Project workflow.

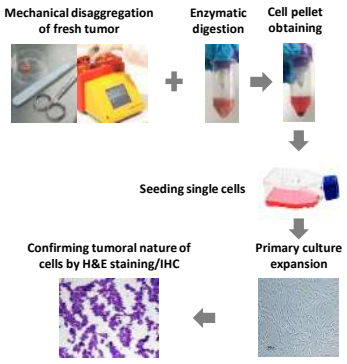

Figure 2. Diagram of patient-derived primary cultures establishment from fresh tumor.

Results

1. Public data analysis of Wnt signalling pathway molecular alterations in STS

Gene	Alteration frequency	Prevalent alteration type	Prevalent altered sarcoma type	Overall Survival
RSPO2	8%	RNAm high	Dedifferentiated liposarcoma	Lower
RSPO3	8%	RNAm high	Leiomyosarcoma	Lower
FZD8	6%	RNAm high	Synovial sarcoma	Lower
APC	10%	RNAm high	Myxofibrosarcoma	NA
CTNNB1	9%	RNAm and protein high	Leiomyosarcoma	Higher
PORCN	9%	RNAm high	UPS	Lower
RNF43	8%	RNAm high	Myxofibrosarcoma	Lower
ZNRF3	4%	RNAm high	Synovial sarcoma	Lower
LRP5	4%	RNAm high	Leiomyosarcoma	NA
LRP6	7%	RNAm high	Dedifferentiated liposarcoma and UPS	Lower
LGR4	4%	RNAm high	Synovial sarcoma	Lower
LGR5	14%	Amplification	Dedifferentiated liposarcoma	Lower
AXIN2	4%	RNAm high	Leiomyosarcoma	Lower
GSK3B	13%	RNAm high	Myxofibrosarcoma and Synovial sarcoma	Lower
SFRP1	5%	Amplification	Myxofibrosarcoma and UPS	Higher
SFRP2	4%	Amplification	Synovial sarcoma	NA
WNT5A	8%	RNAm high	Synovial sarcoma	NA

Table 1. Study of genetic Wnt signalling pathway alterations in STS and their potential impact on patient survival. Gene alteration frequency, prevalent alteration type, prevalent altered sarcoma type and overall survival data compared to non-altered STS patients were obtained from Sarcoma (TCGA, PanCancer Atlas), n=255 patients/samples through cBioPortal for Cancer Genomics. Abbreviations: UPS (Undifferentiated Pleomorphic Sarcoma), NA (Not Available).

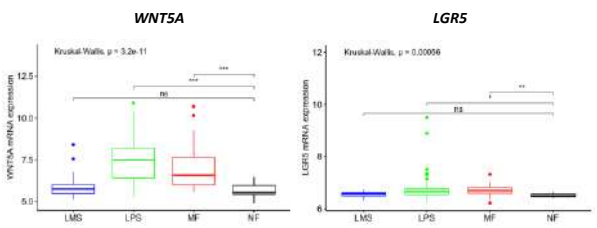

Figure 3. Differences in RNAm expression levels of Wnt pathway members between STS subtypes and non-tumoral samples. Raw data was collected from the National Center for Biotechnology Information (NCBI)/GenBank GEO web site (GSE21122) and normalized in R using Bioconductor and associated packages. For each box plot, median and ranges are indicated. ** p< 0.01 and *** p< 0.001. LMS: Leiomyosarcoma, LPS: Liposarcoma, MF: Myxofibrosarcoma and NF: normal fat.

2. Patient-derived primary cultures: from processed tumours to well-established STS primary cultures

A

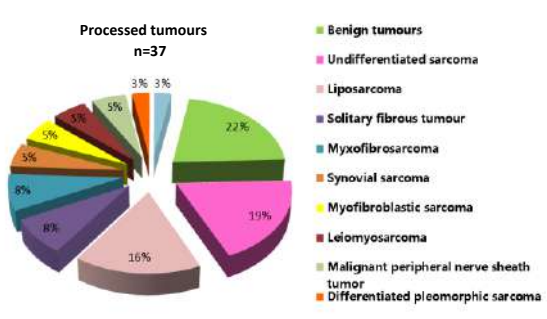

B

ID Primary culture	Tumour histology	Histological grade	Location	Recurrence / Metastasis
MCP016	Undifferentiated pleomorphic sarcoma	High	Lower extremity	No
MCP020	Intramuscular myxoma	-	Lower extremity	No
MCP021	Undifferentiated sarcoma	High	Lower extremity (lymph node)	Metastasis
MCP023	Pleomorphic leiomyosarcoma	High	Upper extremity	No
MCP025	Undifferentiated pleomorphic sarcoma	High	Trunk	No
MCP033	Undifferentiated sarcoma fibrous histiocytoma-like	Intermediate	Lower extremity	Recurrence
MCP036	Myofibroblastic sarcoma	Intermediate	Lower extremity	No
MCP037	Synovial sarcoma	Intermediate - High	Lower extremity	No
MCP038	Dermatofibrosarcoma protuberans	Intermediate	Trunk	No

C

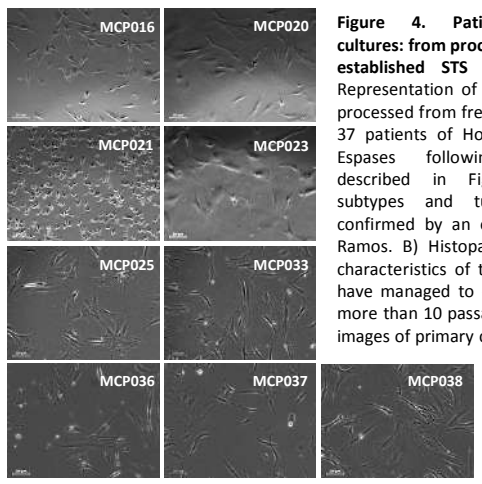

Figure 4. Patient-derived primary cultures: from processed tumours to well-established STS primary cultures. A) Representation of different STS subtypes processed from fresh resected tumours of 37 patients of Hospital Universitari Son Espases following the procedure described in Figure 2. Histological subtypes and tumour grades were confirmed by an expert pathologist, Dr. Ramos. B) Histopathological and clinical characteristics of the 9 tumours that we have managed to establish in culture for more than 10 passages. C) Representative images of primary cell cultures at passage 10 taken with phase-contrast microscope Cell Observer (Carl Zeiss, Germany) with a 10X objective.

3. Characterization of Wnt pathway molecular alterations in patient-derived primary cultures

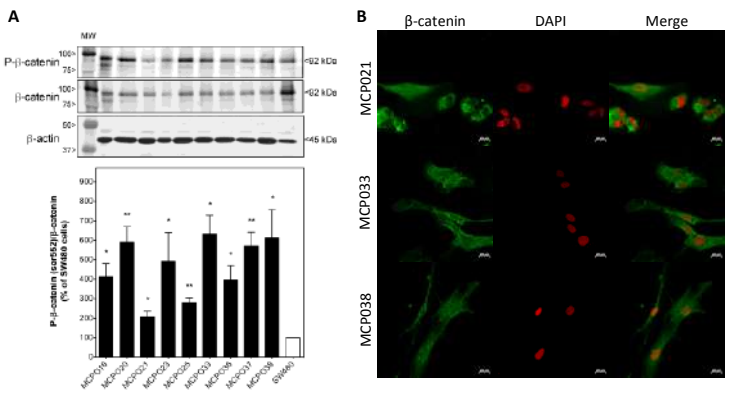

Figure 5. Canonical Wnt signalling is activated in STS primary cultures. A) Upper panels show representative immunoblots of phosphorylated (P-Ser552) and total β-catenin in whole cell-extracts of primary cell cultures. β-actin was used as a loading control. Columns represent the ratio of P-β-catenin (Ser552) to β-catenin immunoreactivity. Each column represents mean ± SEM of 3 independent experiments normalized to SW480 cells (taken as 100%), a human colon cancer cell line used as positive control. *P < 0.05 and **P < 0.01 and ***P < 0.001. B) Subcellular localization of β-catenin (Cell Signaling, #8480) in STS primary cells. Cells were fixed in methanol:acetone (1:1) and Alexa488 was used as secondary antibody. DAPI was added to visualize the nuclei.

Figure 6. Wnt target genes expression in primary cultures. Relative expression of *CDC25A*, *CUL4A*, *AXIN2* and *WNT5A* assessed by qPCR. Each column is one experiment normalized to hMSC (human mesenchymal stem cell line). HT29 (human colon cancer cell line) and PC-9 (human lung adenocarcinoma cell line) were used as positive controls. β-2-microglobulin was used as loading control.

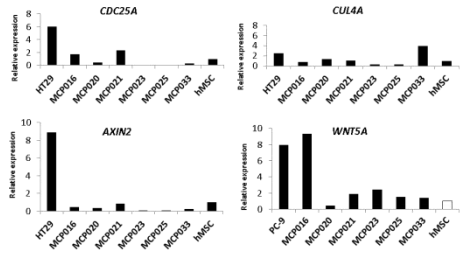

A

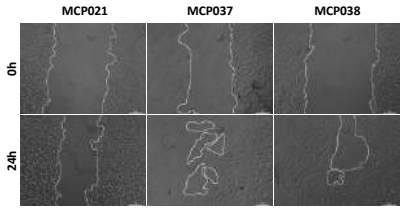

B

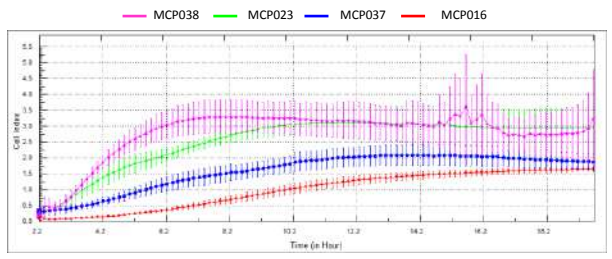

Figure 7. Migration assays in STS primary cultures. A) Wound healing assay showing wound closure of primary cells 24h after the scratch was made. Images were taken with phase-contrast microscope Cell Observer (Carl Zeiss, Germany) with a 5X objective at the same point at 0 and 24h. Free-cell areas are marked in white. B) Real time migration assay using xCELLigence System. The diagram shows a slope (cell index vs. time) of cells that migrated from the upper to the lower chamber.

Conclusions

- ✓ We have set up a protocol for the establishment of patient-derived primary cultures with 33% efficiency, as previously described in other series.
- ✓ All STS primary cultures present aberrant activation of canonical Wnt signalling pathway and some of them show other molecular alterations such as high expression of *WNT5A* at RNAm level. Further genomic characterizations will be performed to complete cell cultures profiles.
- ✓ The detection of oncogenic Wnt signalling pathway alterations in our patient-derived primary cultures will allow us to test different Wnt targeted therapies depending on the specific alteration of each tumor in a personalized approach.

marina.perez@ssib.es

San Espases hospital universitari
Institut d'Investigació Sanitària Illes Balears
GEIS
Fundación Mari Paz Jiménez Casado

A drastic shift in lipid adducts in colon cancer detected by MALDI-IMS lead to the identification of a novel pharmacological target related with 3 consensus molecular subtypes.

Jone Garate[4], Albert Maimó-Barceló[1*], Joan Bestard-Escalas[1*], Roberto Fernández[4], Karim Pérez-Romero[1], Marco Martinez[1,2], Mª Antònia Payeras[1,3], Daniel H. Lopez[1], José Andrés Fernández[4], and Gwendolyn Barceló-Coblijn[1,**]*

[1]Health Research Institute of the Balearic Islands (IdISBa); [2]Pathological Anatomy Unit, Hospital Universitari Son Espases (HUSE) [3] Gastroenterology Unit, HUSE, Palma, Spain; 4Univeristy of the Basque Country, Leioa, Spain.

Introduction and Aims: Colorectal cancer (CRC) is the 3rd most common cancer and is the 4th main cause of cancer death worldwide. Even though is one of the most preventable cancers, it is currently one of the deadliest. Incidence in people <50 years has unexpectedly increased in a significant manner for causes still unknown. Thus, it is imperative to improve prevention and treatment strategies. The application of bioinformatic analysis to large transcriptomic databases has enabled more accurate classification systems in order to better understand the different subtypes of CRC getting closer to a more personalized treatment. In this context, the application of imaging mass spectrometry analysis (IMS) has the potential to unveil more specific information regarding the impact of CRC on the lipidomic profile[1,5] (FIG 1).

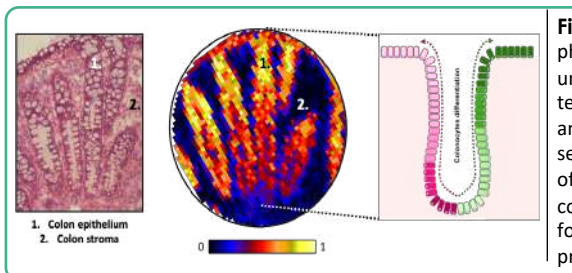

Figure 1. Strict regulation of phospholipid metabolism unveiled using IMS techniques. The detailed analysis of human colon sections shows that the level of a subset of lipids changes concomitantly along the crypt following the differentiation process. Adapted from [4].

Materials and methods: Healthy and adenomatous (AD) human colon biopsies were obtained in the endoscopic room of hospital universitari Son Espases (IB 2118/13 PI). Histological sections (10 µm) were prepared using a cryostat (CM3050S, Leica), and the lipidome was analyzed in positive ion-mode MALDI–IMS, at a 10-15 µm of lateral resolution[1-5] FIG 2. Then, publicly available CRC transcriptomic databases (GSE44076, GSE39582, GSE20916, GSE97689, GSE5206, and TCGA-COADREAD) were interrogated using transcriptomic analysis console (Affymetrix), GEO2R (NCBI) and Xenabrowser (USCS)[6,7]. MTT and clonogenic assays were performed on HT29 and SW480 CRC commercial cells, treated with 3,4-dihydroxyphenylacetic acid (DOPAC, 500 µM) and PF-05089771 (200 nM) inhibitors of K+ and Na+ channels.

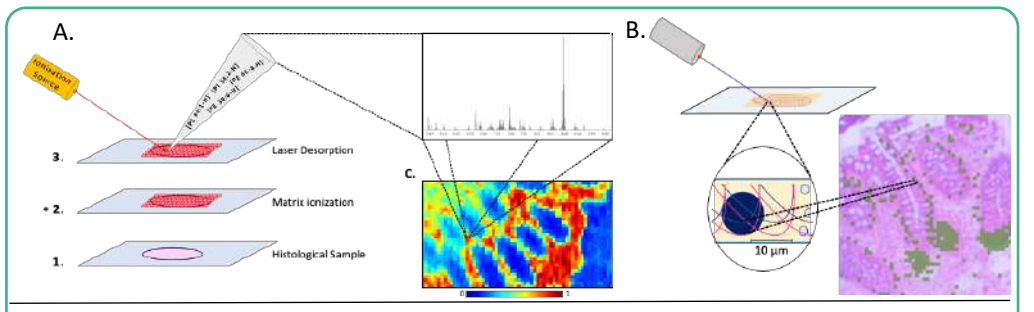

Figure 2. A. Scheme for MALDI-IMS data and imaging generation. **B.** Model for enhanced lateral resolution by using oversampling MALDI-IMS on human colon histological sections. Adapted from [4, 5].

Results: Using MALDI-IMS, we demonstrated a drastic shift of the Na+/K+ lipid adducts ratio when comparing colon AD mucosa to healthy mucosa (FIG. 3.A), strongly suggesting a robust increase in K+ tissue levels (FIG. 3.B). We hypothesized that this shift was a consequence of an altered function of the ion channels accounting for the transport of Na+ and K+. Interrogation of publicly available CRC transcriptomic databases lead to the identification of various K+ and Na+ channel subunits as potential regulators for the observed phenotype (FIG. 4.A). Among them, *KCNAB2* (Voltage-Gated K+ Channel Subunit Beta-2) showed a strong association between gene expression levels (FIG. 4.B) and CRC poor prognosis (FIG. 4.F) and also a high association with 3 CRC subtypes[6] (CMS 4-Mesenchymal, CMS1-MSI Immune and CMS2-Canonical) covering approx. the 70% of CRC heterogeneity (FIG. 4.C). We further investigated the potential role of KCNAB2 as therapeutic target, exploring the impact of its pharmacological inhibition on commercial CRC cell growth. Finally, MTT survival and clonogenicity assays results showed that the pharmacological inhibition of KCNAB2 (DOPAC) drastically halts colon cancer proliferation (FIG. 5).

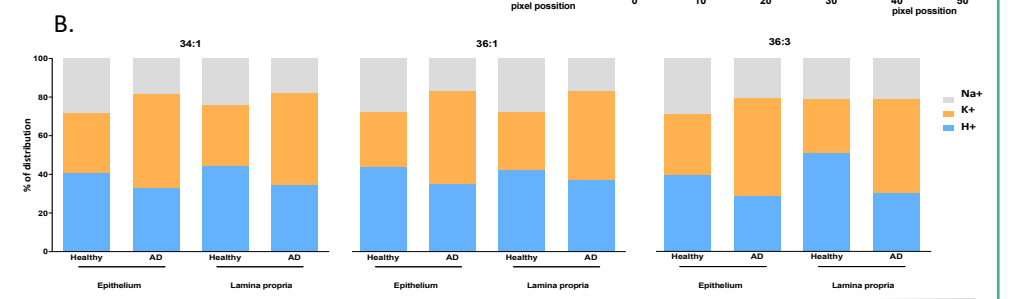

Figure 3.A. Representative distribution of lipid adducts, and Na^+/K^+ ratios, along the crypt axis for epithelium and stroma areas in healthy and adenomatous human colonic samples. **B.** Proportion of lipid adducts (PC 34:1, PC 36:1, PC36:3) for healthy and adenomatous samples in epithelium and stroma areas. A consistent increase in K+ adducts in adenomatous samples is observed in both A and B representations.

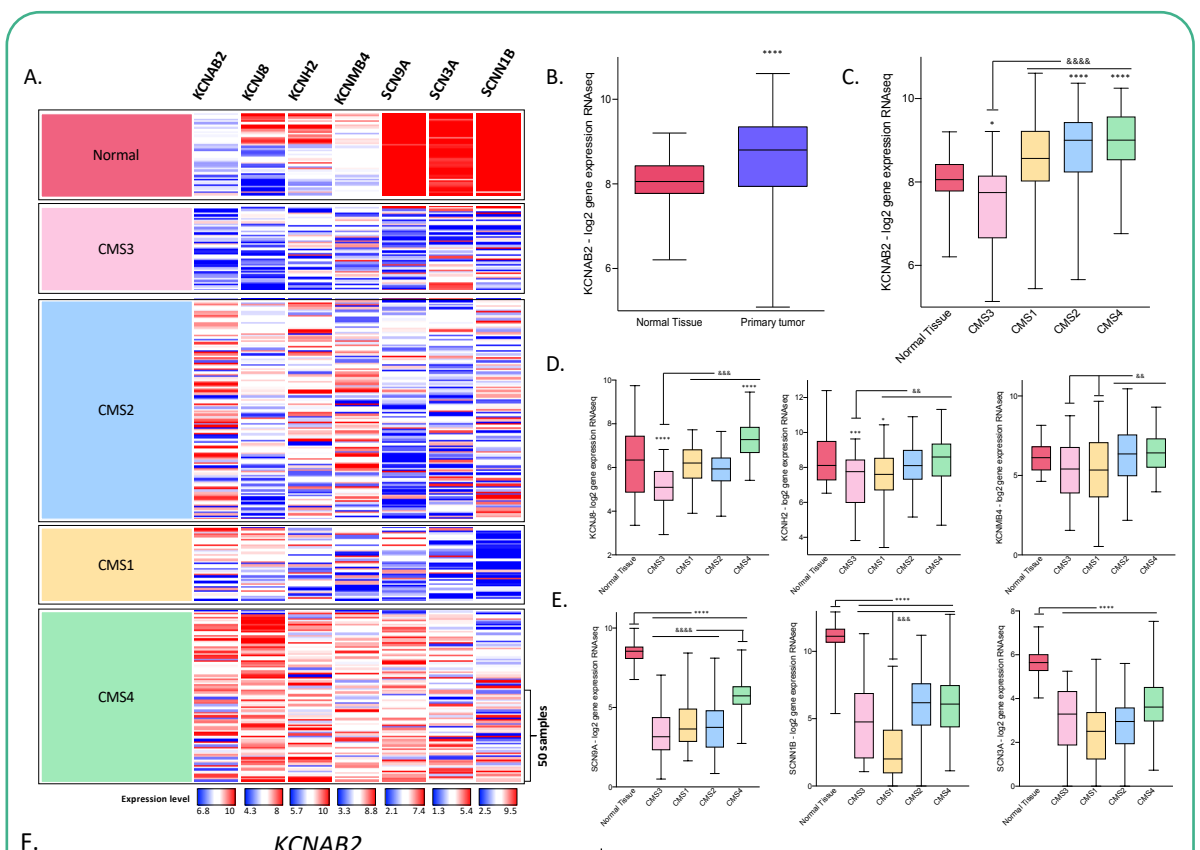

Figure 4. A. Expression level heat-map of selected genes in primary tumors and control samples, and CMS-sample association. Data was visualized with Xenabrowser (USCS)[7] using COADREAD database (TCGA). **B.** *KCNAB2* tumor up-regulation box-plot, **** P < 0.0001, unpaired t test with Welch's correction. **C.** *KCNAB2* high expression associates with CMS1, 2 and 4, P < 0.0001. *KCNJ8, KCNH2, KCNMB4* (**D**) *SCN9A*, *SCN3A* and *SCNN1B* (**E**) gene expression box-plots relative to CMS association. **F.** Kaplan-Meier curves for overall and disease specific survival relative to *KCNAB2* primary tumor gene expression (COADRED database). * P < 0.05, ** or && P < 0.005, *** or &&& P =0.001, **** or &&&& P < 0.0001; "*" is referred to normal tissue, "&" to the marked CMS. Multiple comparisons ordinary one-way ANOVA was used for **C - E**.

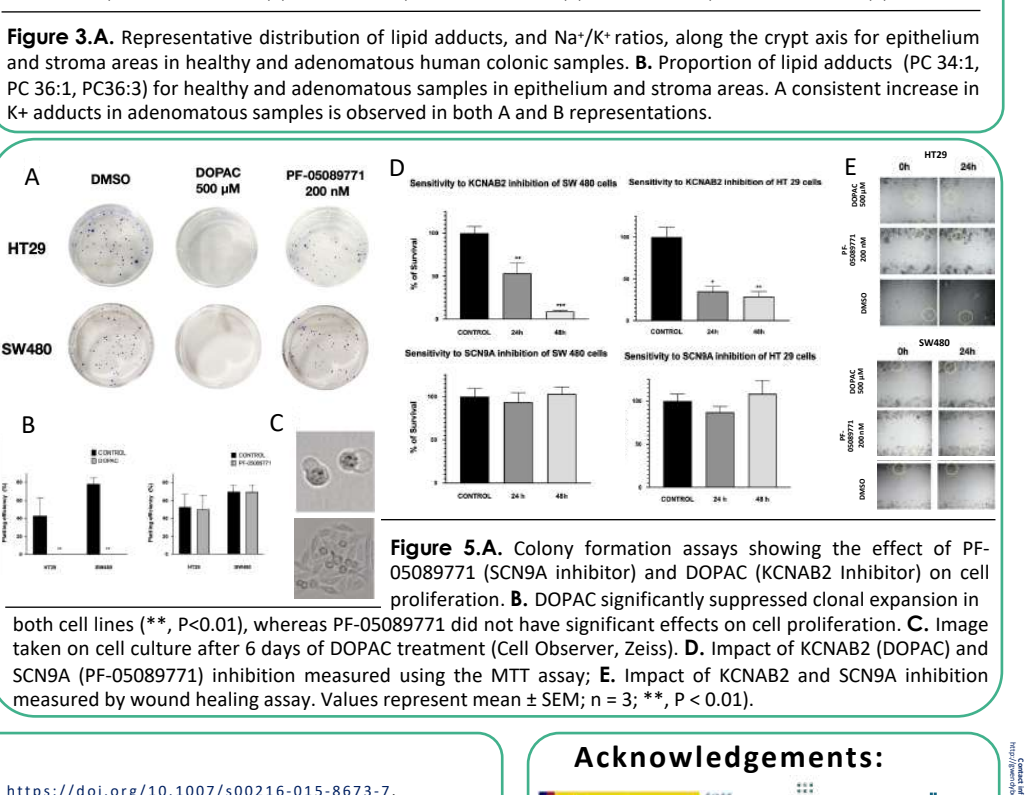

Figure 5.A. Colony formation assays showing the effect of PF-05089771 (SCN9A inhibitor) and DOPAC (KCNAB2 Inhibitor) on cell proliferation. **B.** DOPAC significantly suppressed clonal expansion in both cell lines (**, P<0.01), whereas PF-05089771 did not have significant effects on cell proliferation. **C.** Image taken on cell culture after 6 days of DOPAC treatment (Cell Observer, Zeiss). **D.** Impact of KCNAB2 (DOPAC) and SCN9A (PF-05089771) inhibition measured using the MTT assay; **E.** Impact of KCNAB2 and SCN9A inhibition measured by wound healing assay. Values represent mean ± SEM; n = 3; **, P < 0.01).

Conclusion:

- These results remarks the versatility of lipidomic MALDI-IMS to study tissue molecular alterations.
- MALDI-IMS lead to the identification through publicly available transcriptomic databases of KCNAB2 as a novel CRC target.
- The pharmacological inhibition of KCNAB2 open the door to further investigate the on more complex experimental models.

References :

1. Garate, J. *et al.* 2015. https://doi.org/10.1007/s00216-015-8673-7.
2. Bestard-Escalas, J. *et al.* 2016. https://doi.org/10.1016/j.bbalip.2016.09.013.
3. López, D.H. *et al.* 2018. https://doi.org/10.1016/j.bbalip.2018.04.017.
4. Bestard-Escalas, J. *et al.* 2019. https://doi.org/10.1016/j.jmb.2019.08.006.
5. Maimó-Barceló, A. *et al.* 2019. https://doi.org/10.1007/s00216-019-02212-3.
6. Guinney, J. *et al.* 2015. https://doi.org/10.1038/nm.3967.
7. Goldman, M.J. *et al.* 2020. https://doi.org/10.1038/s41587-020-0546-8.

Acknowledgements:

ZERO TOLERANCE TO SCIENTIFIC FRAUD
STOP IT. REPORT IT

Deciphering the potential of tumor-infiltrating circulant immune cells lipidomic characterization in CRC.

Karim Pérez-Romero[1], Albert Maimó-Barceló[1], Ramón M Rodríguez[1], Paloma de la Torre[3], Lucía Martín-Sáiz[2], José Andrés Fernández[2] Gwendolyn Barceló-Coblijn[1], Daniel H. Lopez[1]

1. Balearic Islands Health Research Institute (IdISBa), Spain; 2.Dep. of Physical Chemistry, University of the Basque Country (UPV/EHU), Leioa, Biscay, Spain; 3.Gastroenterology Unit, Hospital Universitari Son Espases, Palma, Balearic Islands, Spain

Introduction & Aims

Despite progress made in the colorectal cancer (CRC) field, the increase of the overall survival for patients in advanced stages remains still elusive. Therefore, besides improvements in the identification of emerging biomarkers for early detection, the development of new patient stratification tools and new immunotherapeutic treatments for the disease becomes essential. Remarkably, several studies have shown that the tumor microenvironment (TME) plays a crucial role in CRC progression. In this context, this study aimed to lay the groundwork for the characterization of the membrane lipid fingerprint of circulating immune cells of healthy donors and CRC patients, which eventually may infiltrate the tumor and play a pivotal role in tumor immunosurveillance.

Methods

The sample collection for this study was specifically approved by the Ethics Research Committee of the Balearic Islands (IB 3587/17 PI). Blood samples were obtained from 5 CRC patients and 5 control patients, enrolled at the Gastroenterology Services (IB 3350/16).

Peripheral blood immune cells were obtained after blood centrifugation. Subsequently, circulating $CD3^+/CD4^+$ (CD4+ Lymphocyte),$CD3^+/CD8^+$ (CD8+ Lymphocyte),$CD3^-/CD56^+$ (NK Cell),$CD3^+/CD56^+$ (NKT Cell),$CD3^-/CD14^+$ (Monocyte), $CD66b^+$ (Neutrophil) and $CD3^-/CD19^+$ (B Cell) cells were isolated by Fluorescent Activated Cell Sorting (FACS).

Sorted immune cells (100.000 cells) were applied on poly L-lysine coated glass slides and analyzed by Matrix-Assisted Laser Desorption Ionization mass spectrometry (MALDI-MS).

Results

Using the methodology developed to apply the cells on the poly-L-lysine we were able to establish the lipidome using at least 1 to 2 orders of magnitude fewer cells than it is usually used. The analysis allowed the characterization of the main membrane lipid species within circulating monocytes, NK cells, B and T lymphocytes, neutrophils, and NKT cells. First, such analysis revealed a distinctive pattern of lipid species distribution for every cell type, confirming the specificity of the lipid fingerprint and the accuracy of the lipidome for our proposal to describe the immune compartment that shapes the TME.

Furthermore, the comparison between the healthy controls and CRC patients revealed a significant turnover of arachidonic acid-containing phosphatidylethanolamine (PE) and PE-plasmalogens, that may be associated with the clinical condition.

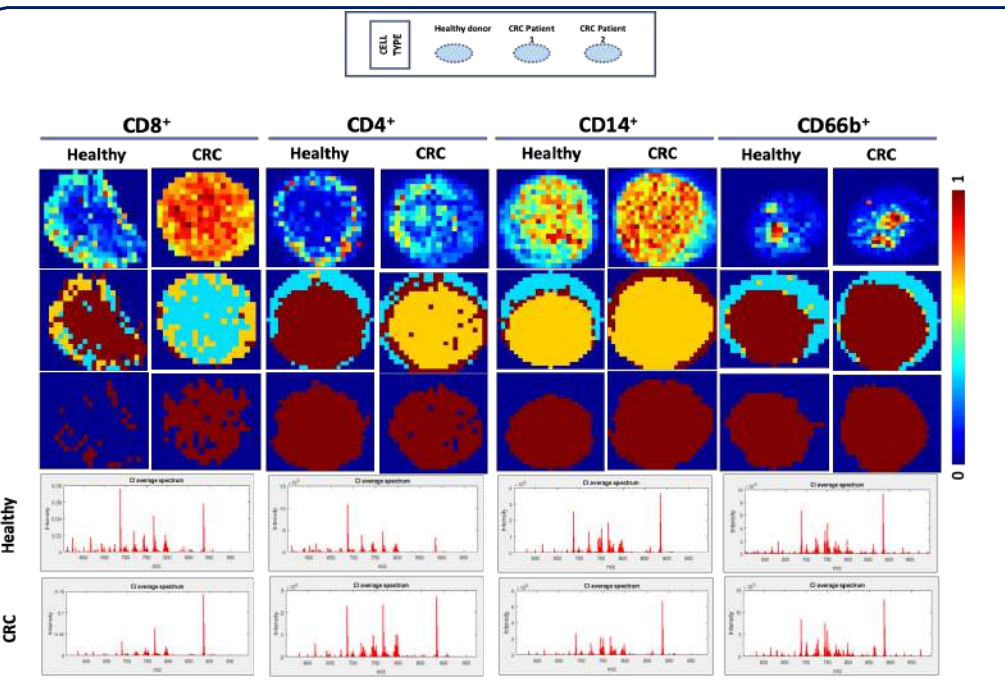

Figure 1. MALDI-IMS representation of the samples seeded overlapping drops on 0.2% poly-L-lysine coated slides. Images from the top row represent the isotopic distribution of the lipid 885.55 m/z in each droplet, providing information of its intensity along the sample. The middle row shows a non-supervised HD-RC Clustering (set at 3 clusters). Pixels are grouped based on their similarity, providing information about how the intensity of the signal is distributed along the droplet, which may correlate with the areas with a higher cell density. The bottom row shows the chosen cluster for each sample, which is the one that exhibits the most lipid-enriched average spectrum of the generated clusters.

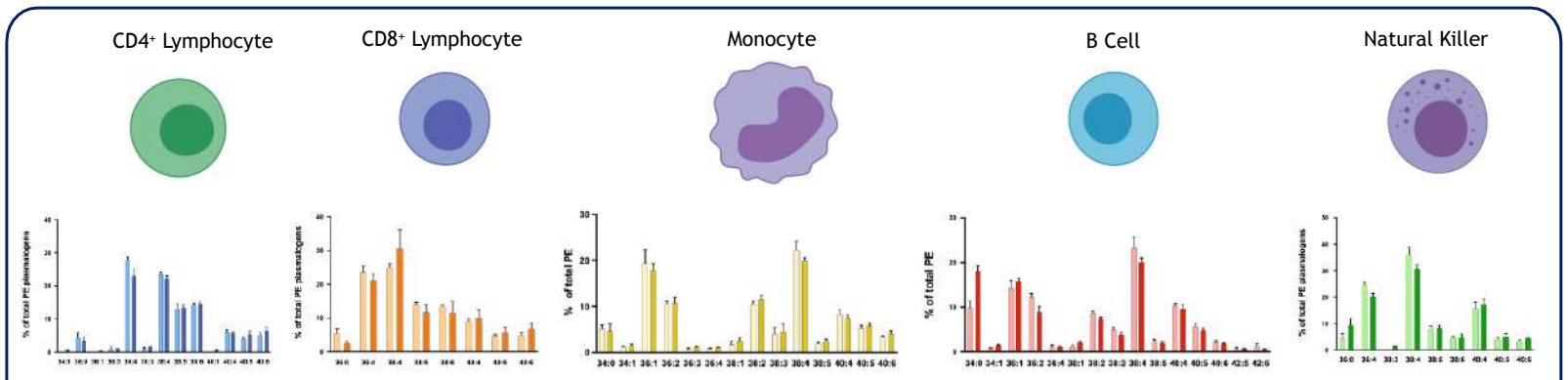

Figure 2. Membrane lipid composition of peripheral blood immune cells isolated from healthy donors and CRC patients. This data exhibit the significant changes detected in the lipid species composition within the PE and PE plasmalogens lipid classes under health conditions and in colorectal cancer disease. These changes are consistent with previous results published by our group, in wich a turnover of arachidonic acid-containing species has been documented in the lamina propria in the context of CRC[1,2]

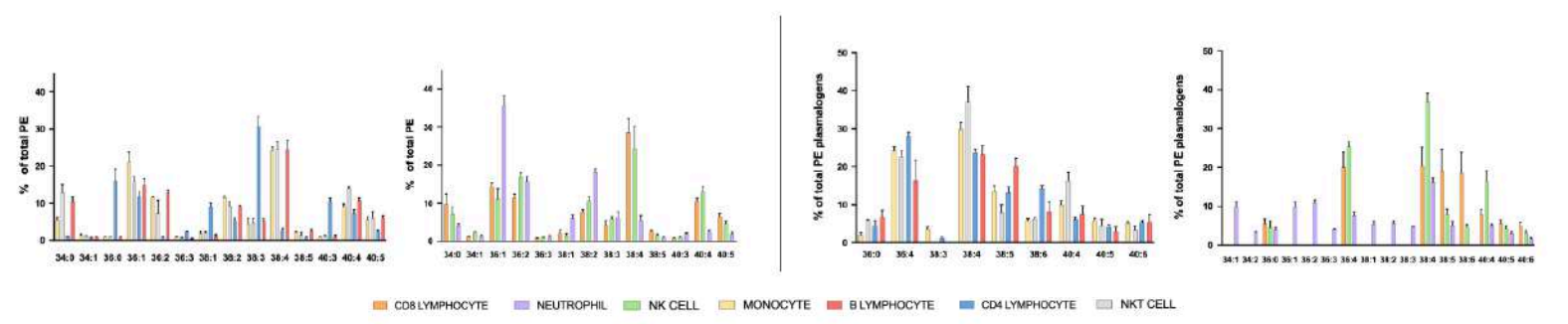

Figure 3. Membrane lipid composition in % of PE plasmalogens and PE for each of the isolated circulating-immune cell types. This representation illustrates the suitability of the lipid fingerprint for a thorough characterization of the TME, given that each immune cell type appears to present their intrinsic proportion of the main lipid species within these lipid classes.

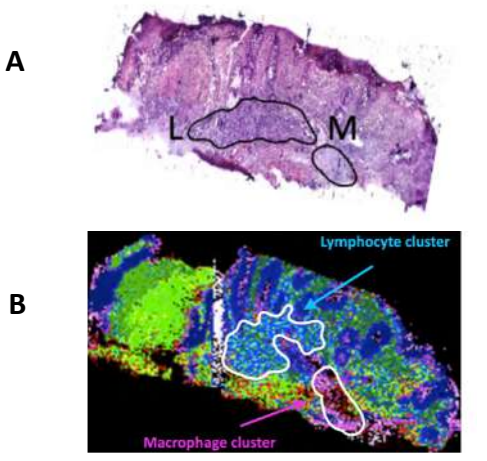

Figure 4.Histological section of inflammed colon mucosa (ulcerative colitis patient). A. Hematoxilin and eosin stain betraying the presence of lymphocytic (L) and macrophage (M) infiltrates. **B.** MALDI-IMS analysis of the consecutive section revealed lipid clusters associated to each cell type, reinforcing the potential of the lipid fingerprint as a suitable tool to study the TME in colorectal cancer disease.

References

1. Bestard-Escalas, J., Garate, J., Maimó-Barceló, A., Fernández, R., Lopez, D. H., Lage, S., ... & Amengual, I. (2016). Lipid fingerprint image accurately conveys human colon cell pathophysiologic state: A solid candidate as biomarker. Biochimica et Biophysica Acta (BBA)-Molecular and Cell Biology of Lipids, 1861(12), 1942-1950.

2. Lopez, D. H., Bestard-Escalas, J., Garate, J., Maimó-Barceló, A., Fernández, R., Reigada, R., ... & Barceló-Coblijn, G. (2018). Tissue-selective alteration of ethanolamine plasmalogen metabolism in dedifferentiated colon mucosa. Biochimica et Biophysica Acta (BBA)-Molecular and Cell Biology of Lipids, 1863(8), 928-938.

Conclusions

- **The setting up of this methodology has finally allowed the lipidomic characterization of sorted immune cells. Consequently, the increase in the sample size will have a direct impact on the robustness and the reliability of the results**
- **The molecular species relative abundance are intrinsic of each immune cell type, that is profoundly affected in patients with CRC. The methodology we have developed allows analyzing a smaller quantity of cells, providing the unique chance to analyze the lipidome of minor subsets of immune cells for the first time.**
- **The spatial resolution of MALDI-IMS allows the localization of lipid clusters that can be associated to specific cell types and its activation state, opening chances to an unprecedent level of detail in a single histological section**

Acknowledgements

We are greatly thankful to the nurses and medical doctors of the Gastroenterology Unit of the Hospital Universitari de Son Espases (Palma, Spain).**Funding**: Institute of Health Carlos III (Miguel Servet Program, CP12/03338 & PI16/02200), Govern Balear (FPI/1787/2015), MINECO (RTC-2015-3693-1), Asociación Española Contra el Cáncer, Junta de Baleares(AECC 02/2017) co-funded by **European Regional Development Fund.**

Contact information: karim.perez@ssib.es http://gwendybc22.wixsite.com/lipidshumanpathology